Chapter 1 Introduction

1.1. 'You cannot connect the dots looking forwards, you can only connect them looking backwards.'

This thesis details the investigations of two separate topics: gold nanoparticles and nitroxide-based polymerization inhibitors. Due to funding arrangements, the two topics are relatively unrelated. However, a major bridge linking the projects is that the aims and methods used in the investigations make the two projects both fall into the 'physical organic' category. The term 'physical organic' was introduced in 1940s, which refers to the study of structure, reactivity, mechanism and their inter-relations. In this thesis, neither of the projects is very application-driven. The big question for the projects was always 'what happened' rather than 'what it can be used for'. Evidently, human beings would have lived much more miserably if more efforts had been made to understand 'which came first, chicken or egg' rather than developing medicine and new materials. Luckily, the history of science research is full of 'happy accidents'. For instance, the concept of 'perpetual motion machine' was proved physically impossible. However, on the way of pursuing such an idealized model, more than 100 useful machines were built, which brought substantial benefits to human being. The purpose of addressing the happy accidents is to emphasize mechanistic studies. A well-known example of the happy accident is the discovery of penicillin by Alexander Fleming in 1928. However, as early as 1590, one of the greatest physicians and pharmacologists in Chinese history, Li Shizhen, described a 'mouldy residue of tofu' that could be used to treat malignant sore and swelling in his epic book 'Compendium of Materia Medica'. During the following hundreds of years, the nature of his observation was never understood and the active ingredients were never isolated. This is an example of how a happy accident could have saved countless lives during more than 300 years and was buried due to technical limitations and more importantly, a lack of mechanistic studies. Mechanistic investigations enhance people's understanding of Nature. However, very often the understanding does not lead to immediate applications, in many cases it even fails to

predict a future application. The development of the applications can thus only be connected to the mechanistic investigations backwards, but rarely forwards. Steve Jobs, CEO and co-founder of Apple Computer, told a story in his speech at the Stanford commencement in 2005, about his interest in the 'not so useful' calligraphy turned into a priceless asset when he designed the first Macintosh computer 10 years later. He commented 'you cannot connect the dots looking forwards, you can only connect them looking backwards'. His speech not only encouraged Stanford graduates and the young generation of entrepreneurs, but also inspired a student in chemistry research across the ocean.

The projects investigated in this thesis were challenging and interesting. In order to solve the complicated problems, a number of analytical methods were required. Among these methods, Electron Paramagnetic Resonance was used heavily in the kinetic and mechanistic studies. Next section considers the principles of continuous-wave Electron Paramagnetic Resonance spectroscopy. Since the investigations described in this thesis do not involve complicated spin systems and analysis of complex spectra, mathematical descriptions (*e.g.* spin Hamiltonian, Bloch equations, magnetization) are kept to minimum.

1.2. Electron Paramagnetic Resonance Spectroscopy

1.2.1. Basic principles of Electron Paramagnetic Resonance

Election Paramagnetic Resonance (EPR) spectroscopy,[1-2] which is also known as Electron Spin Resonance (ESR) spectroscopy, studies paramagnetic species that have one or more unpaired electrons. EPR spectroscopy has been applied to different disciplines and research areas including physics, chemistry, biology, medicine and geology since it is a most direct and sensitive method to study paramagnetic species.

Single electron has spin angular momentum S=1/2 and spin quantum number $m_s = \pm 1/2$ (spin "up" and "down"). In the presence of an external magnetic field H_0,

the magnetic moment can align itself either parallel or anti-parallel to the magnetic field. Therefore the external magnetic field H_0 splits the two degenerate spin states, α and β. This effect is known as Zeeman splitting (Figure 1.1).

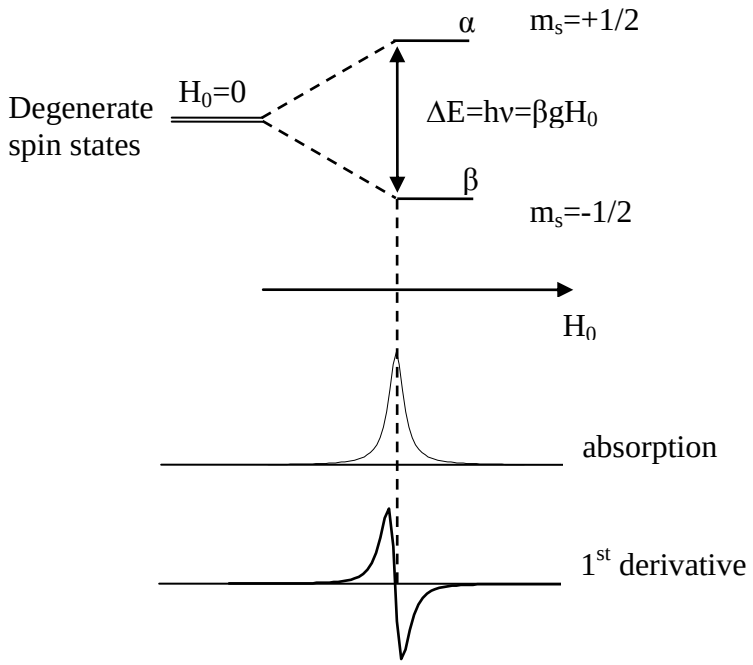

Figure 1. 1. Zeeman effect.

Spin Hamiltonian can be used to describe spin states. For a single electron in vacuum, the spin Hamiltonian H can be written as Equation 1.1.

$$H = |\beta| \vec{g} \vec{H} S \tag{1.1}$$

Here β is the Bohr magneton of the electron, g is the electron g-factor (for free electron g_e is 2.002319), $\vec{H}$ is the external magnetic field vector and S is the electron angular momentum. Irradiation with appropriate frequency can cause the spins to flip from one state to the other. The EPR selection rule is $\Delta m_s = \pm 1$, therefore the energy separation of the lower spin state (parallel alignment) and the upper spin state (anti-parallel alignment) can be described in Equation 1.2.

$$\Delta E = \beta g H_0 = h\nu \tag{1.2}$$

Here, ν is the radiation frequency and h is the Planck constant. When Equation 1.2 is fulfilled, free electron absorbs energy and flips from the lower energy spin state to the higher energy spin state, which is the effect of paramagnetic resonance.

1.2.2. Detection of resonance

The resonance condition depends on two factors, the external magnetic field H_0 and the frequency of microwave radiation ν. Therefore, there are two ways to perform an EPR experiment, field sweep and microwave frequency sweep (Figure 1.2).

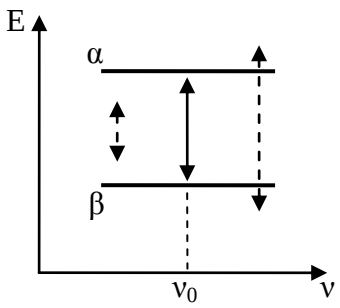

Frequency sweep - to keep H_0 constant and vary radiation frequency ν.

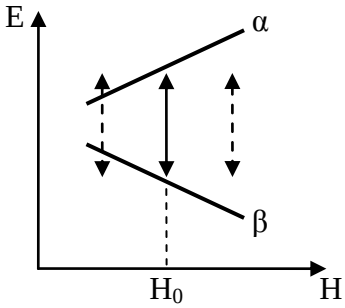

Field sweep - to keep ν constant and vary external magnetic field H.

Figure 1. 2. Two ways of performing EPR experiments: frequency sweep and field sweep[3].

In this work, the sample (electron spins) was irradiated with a microwave radiation at fixed frequency in the ~9.75 GHz (known as X-band) region and the magnetic field was swept. The method is often referred to as continuous wave EPR (cw-EPR) Spectroscopy.

The frequency of the microwave radiation stipulates EPR wavebands (Table 1.1). Higher frequency brings the EPR spectra to higher magnetic field. As a result, species with slightly different g values can be better distinguished. An X-band spectrometer was used in this study since it is adequate for the analysis of most organic radicals.

Table 1. 1. EPR wavebands.

Frequency region/GHz	EPR waveband	Resonance field/G
~1.1	L-band	~392
~3.0	S-band	~1070
~9.75	X-band	~3480
~34.0	Q-band	~12000
~94.0	W-band	~34000

1.2.3. EPR Instrumentation

The instrument[3] setup of an X-band EPR spectrometer is shown in Figure 1.3.

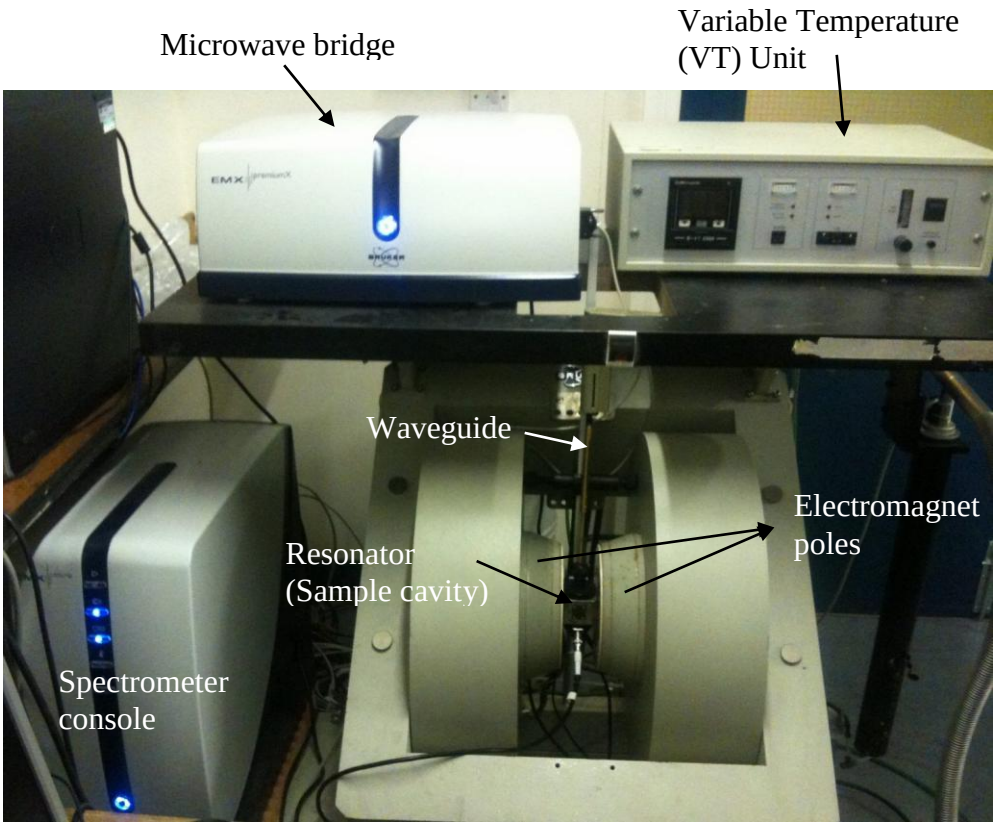

Figure 1. 3. Bruker EMXmicro CW-EPR spectrometer.

The microwave radiation generated in the microwave bridge travels down the waveguide to the resonator which is located between the two magnet poles. The magnetic field is scanned while the absorption of microwave radiation is measured. The signal is processed in the spectrometer console and EPR spectra are thus obtained. In order to increase the signal-to-noise ratio (SNR), the magnetic field is

modulated by the modulation circuit on the sides of the resonator, leading to 1st derivative EPR spectra.

1.2.3.1. Microwave bridge

The microwave bridge is an important component of an EPR spectrometer. As shown in the block diagram (Figure 1.4), a microwave generator (*e.g.* Guun diode or klystron) supplies CW microwave radiation which travels to the sample cavity via a circulator. The circulator directs reflected signal from the cavity to the microwave detector. The detector diode has a linear response region in which accurate measurement of signal intensity is allowed. In order to ensure the detector operates in the linear region, a reference arm is used to control the power level. The bias attenuator adjusts the signal to the appropriate amplitude ratios. Since the detector is phase sensitive, the phase shifter ensures the reference microwave is in phase with the reflected signal from the cavity.

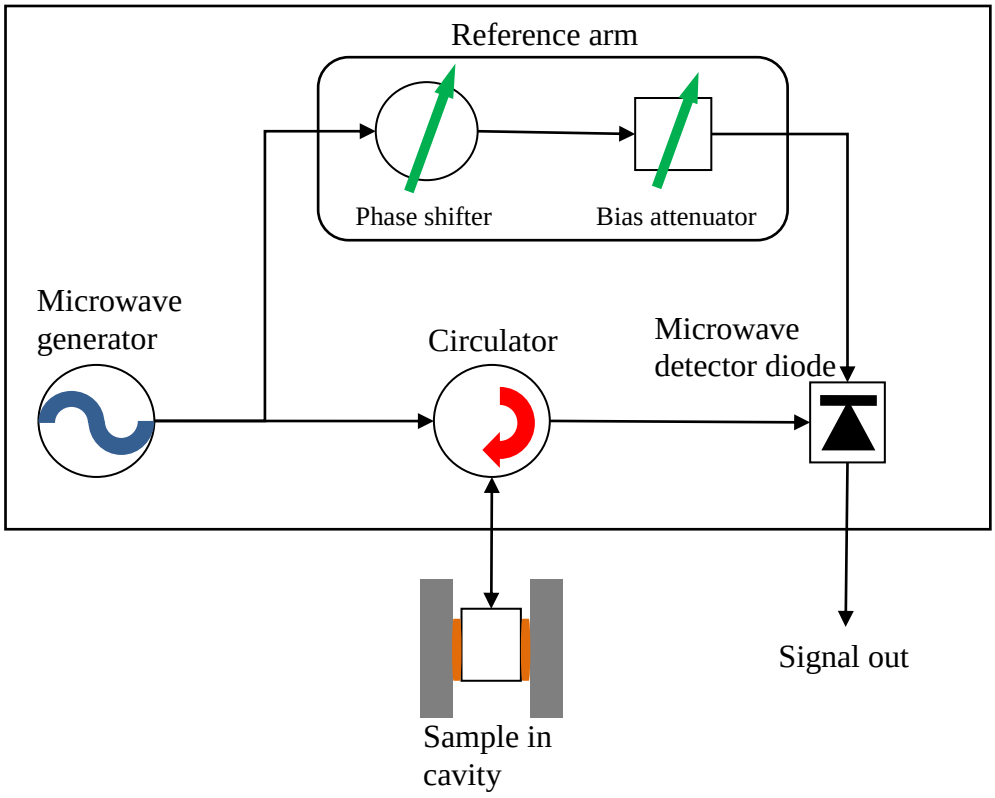

Figure 1. 4. Microwave bridge schematics.

1.2.3.2. Magnetic field modulation

Due to the very short relaxation times of electron spins, it is necessary to enhance the sensitivity of the EPR spectrometer. A phase sensitive detection technique is used to filter out noise and electronic interference. The basic principle is to modulate the magnetic field sinusoidally at a modulation frequency ν_m with amplitude H_m by the circuits on the sides of the resonator. The output amplitude A of the modulation corresponds to the slope of the absorption line at the resonance field, therefore the absorption line is converted to the 1st derivative spectrum (Figure 1.5). In the signal channel, any signals which do not have the same frequency and phase as the field modulation are suppressed. As a result, the sensitivity of EPR spectroscopy is increased by several orders of magnitude. Wise choice of the modulation amplitude and frequency is important for truthful detection of EPR signal, since inappropriate modulation could distort the spectra.

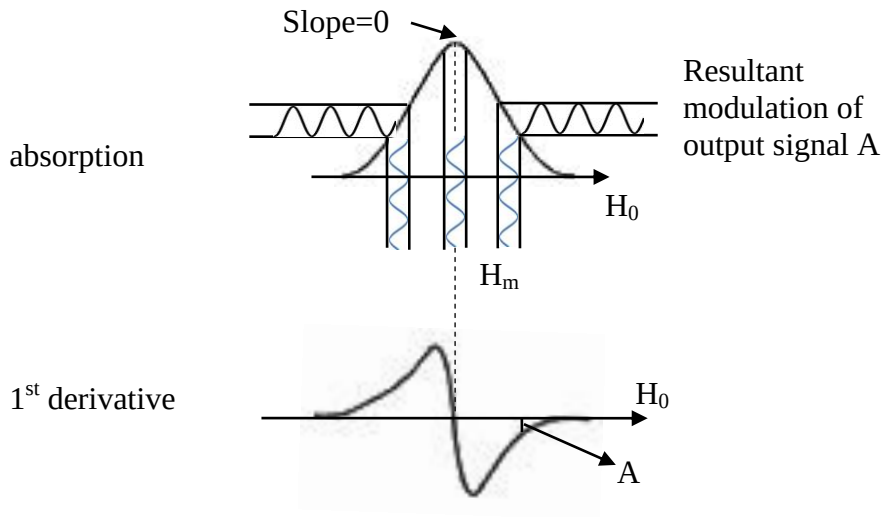

Figure 1. 5. Magnetic field modulation.

1.2.3.3. Variable temperature measurements

A variable temperature (VT) unit is often used to permit EPR measurements at different temperatures. It was essential in our investigations since many of the kinetic studies in this work were undertaken at controlled temperature. The available temperature range of EPR experiments is typically 4-500 K. Low temperature measurements are usually based on overpressure of liquid nitrogen (77 K) or liquid

helium (4.2 K), while high temperature can be achieved by heating of pumped air. A suprasil Dewar insert, which is EPR silent and microwave transparent, is attached to the sample cavity and allows the appropriate gas (*e.g.* air or N_2) to pass through. The heater inside the insert heats the gas and the thermocouple placed near the sample accurately measures the temperature. The heater power is controlled by a VT unit (as shown in Figure 1.3, p5) and thus EPR measurements at the desired temperature can be achieved.

1.2.4. EPR spectral parameters

1.2.4.1. g-factor

The role of g-factor in EPR is similar to chemical shift in Nuclear Magnetic Resonance (NMR). For the unpaired electrons in molecules, the spin-orbit coupling contributes to the angular momentum, which leads to deviation of the g values from g_e of the free electron. For organic radicals, angular momentum is dominated by the contribution from the electron spin, the g values of such radicals are thus very close to g_e. As a result, g-factor is more useful to distinguish different types of paramagnetic species.

It is considered that g-factor is anisotropic due to the anisotropy of spin-orbit interactions. Although the orbit contribution is small for organic radicals, anisotropic g tensor depends on the direction of the magnetic field and orientation of the paramagnetic molecule. Anisotropic g tensor can be measured by rotating a paramagnetic single crystal in the spectrometer and measuring the EPR spectra at different orientations. Equation 1.3 describes the calculation of g values at different orientation.

$$g^2 = \begin{pmatrix} l_x & l_y & l_z \end{pmatrix} \begin{pmatrix} g^2_{xx} & g^2_{xy} & g^2_{xz} \\ g^2_{yx} & g^2_{yy} & g^2_{yz} \\ g^2_{zx} & g^2_{zy} & g^2_{zz} \end{pmatrix} \begin{pmatrix} l_x \\ l_y \\ l_z \end{pmatrix} \tag{1.3}$$

Here, l_x, l_y and l_z represents the cosine of the polar angles of the applied magnetic field H_0 with the molecular axis system. Figure 1.6 depicts a nitroxide radical (discussed in detail in Chapter 3) placed at the xz plane of the polar angles of an external magnetic field H_0 with the molecule.

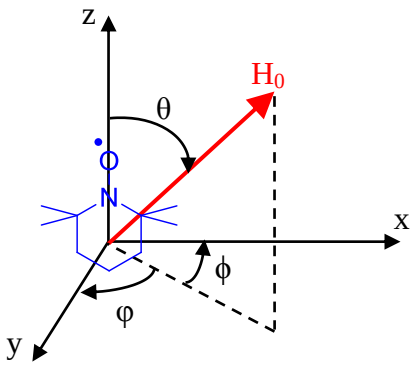

Figure 1. 6. The orientation of the applied magnetic field in the molecular axis system. The nitroxide radical is placed at the xz plane.

In our investigations, the samples were in liquid phase (*e.g.* in solution) and anisotropy of g tensors is averaged out due to rapid tumbling of the molecules. Therefore, in liquid phase EPR spectra appear at isotropic g values g_{iso}.

1.2.4.2. Hyperfine interaction

The unpaired electron is very sensitive to its local surroundings. The interaction between an unpaired electron with nearby nuclear spins is known as hyperfine coupling.

Similar to electrons, nuclei are characterized by spin angular momentum *I* (Table 1.2) and corresponding magnetic moment μ_N. Nuclei which have $I \neq 0$ are magnetic. In the presence of an external magnetic field H_0, the moment of a nucleus has $2I+1$ different alignments, corresponding to nuclear spin quantum number m_I=I, I-1, I-2…, -I, which have different energy states. The transition between the energy states under selection rule of $\Delta m_I = \pm 1$ is known as the Nuclear Magnetic Resonance (NMR).

Table 1. 2. Nuclear spin of isotopes.

Isotope	Nuclear spin *I*
^{1}H, ^{13}C, ^{31}P, ^{15}N	1/2
^{2}H, ^{14}N	1
^{12}C, ^{16}O	0
^{55}Mn	5/2

Nuclear spin interacts with electron spin, and therefore further splits the electron Zeeman sub-levels by the hyperfine coupling constant A. For instance, proton (I=1/2) splits the two Zeeman sub-levels of an unpaired electron into 4 energy states (Figure 1.7). EPR transition between the energy states complies with $\Delta m_s = \pm 1$ and $\Delta m_I = 0$ selection rules under high field approximation (hyperfine is much smaller than electron Zeeman splitting).

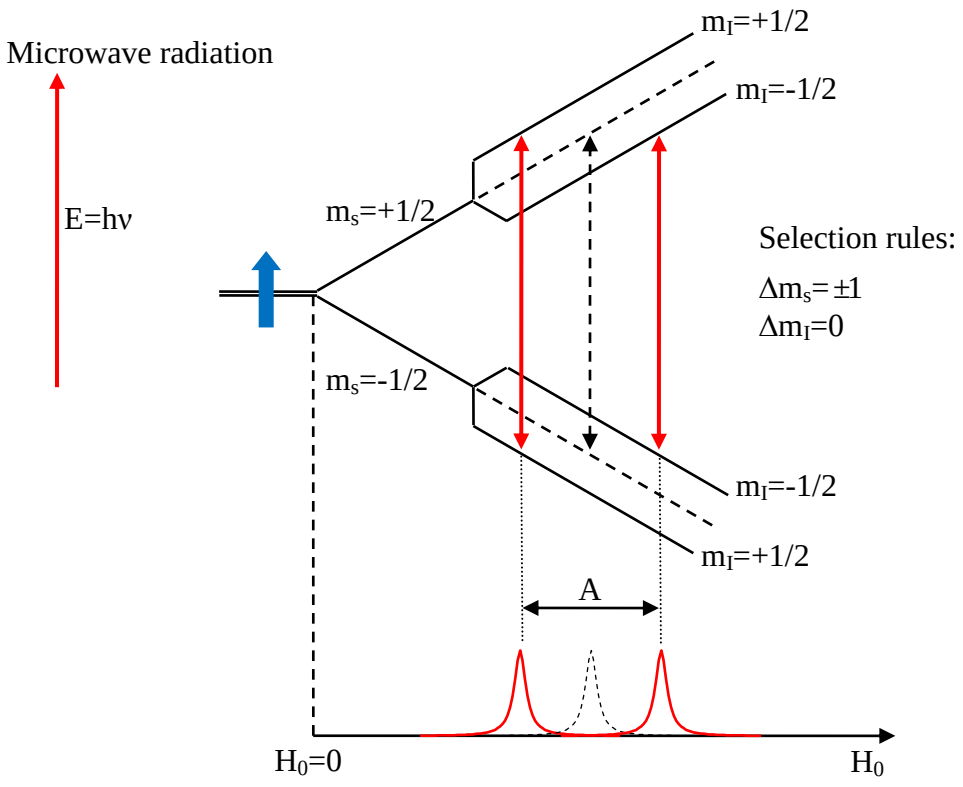

Figure 1. 7. Hyperfine splitting of ^{1}H.

For nitroxide radicals, since ^{14}N has a spin angular moment I=1 and resulting spin quantum number m_I=1, 0 and -1, the degenerate spin state is split into two Zeeman

sub-levels and further split into six energy states. Based on the EPR selection rules $\Delta m_s = \pm 1$ and $\Delta m_I = 0$, there are three allowed transitions leading to a triplet EPR spectrum (Figure 1.8).

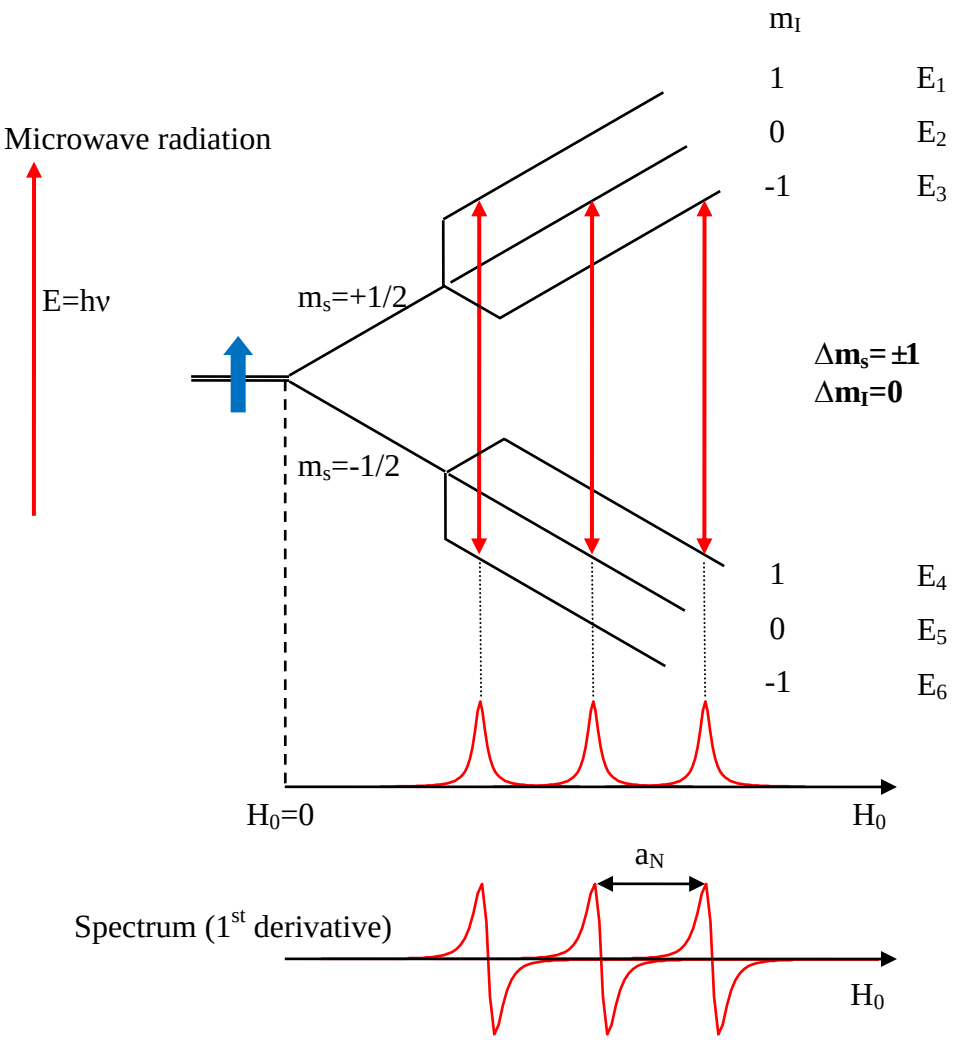

Figure 1. 8. Hyperfine splitting of an unpaired electron by ^{14}N.

Typically, the interactions of an unpaired electron with n equivalent nuclei having nuclear spin *I* lead to $2nI+1$ lines in the EPR spectrum.

Hyperfine splitting is due to the interaction of the unpaired electron with nuclear spins. The nature of the interaction has several contributors.

Electron-nulcear dipole-dipole interaction

Magnetic nucleus provides an additional magnetic field (known as hyperfine field) which is experienced by the unpaired electron. The hyperfine magnetic field is a classic field of a magnetic dipole, therefore the interaction is known as the dipole-dipole interaction. The electron-nuclear dipolar interaction decreases with the increasing electron nucleus distance r, and also depends on the angle between the direction of the external magnetic field H_0 and the orientation of the vector connecting the dipoles (Figure 1.8). Hence, hyperfine is anisotropic. Dipole-dipole interaction is thus very important for solid samples. In an isotropic environment, fast tumbling of the molecules averages out dipolar interaction.

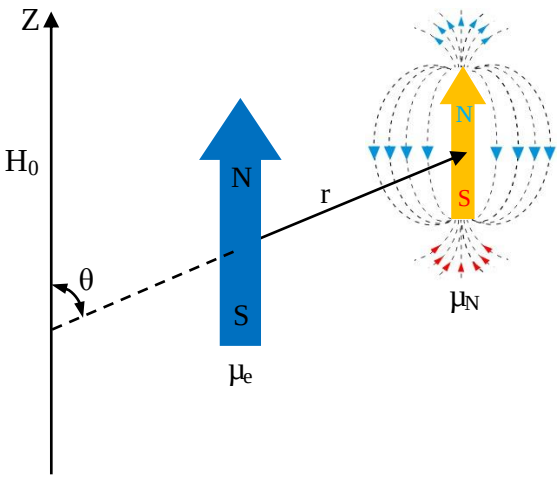

Figure 1. 9. Dipole-dipole interaction.

Fermi contact

Fermi contact originates from the s-electron density at the nucleus. Inside the nucleus the hyperfine field is constant and isotropic. Therefore the contact contribution to the hyperfine is also isotropic. Fermi contact, however, cannot explain the hyperfine coupling between an electron populating a SOMO (Singly Occupied Molecular Orbital) and the magnetic nuclei in an extended π system.

Spin polarization

Spin polarization refers to the tendency of the electron in the SOMO to align its spin with the spin of the nearest nucleus. For instance, there are two possible spin orientations for a C-H bond (Figure 1.10). The spin state in which the SOMO electron is coupled with the spin of H atom is favourable. The resulting hyperfine coupling constants are linearly proportional to the spin density on the 'C' nucleus.

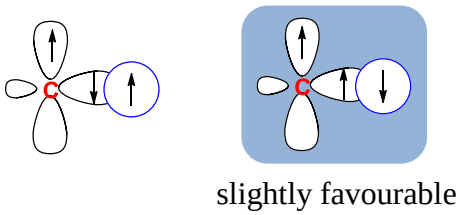

Figure 1. 10. Two possible spin orientations of a C-H bond.

1.2.4.3. Spectral linewidth and intensity

Based on the resonance condition $h\nu=\beta g H_0$, EPR spectra should be monochrome (*e.g.* infinitely narrow lines). In reality, spectra always have a certain width and shape due to different mechanisms. A 1st derivative EPR spectrum is characterized by the peak-to-peak linewidth ΔH_{pp} (Figure 1.11).

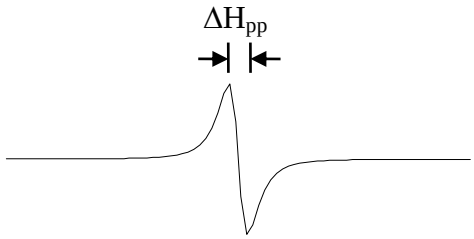

Figure 1. 11. Peak-to-peak linewidth of a 1st derivative line.

The observed spectrum (*e.g.* Voigt shape) can be considered as a convolution of an inhomogeneous contribution and a homogeneous contribution. Inhomogeneous broadening which gives a Gaussian lineshape, often comes from unresolved hyperfine structures, modulation induced spectral distortion and spread in the

magnetic parameters (*e.g.* hyperfine coupling constant A) among different paramagnetic centres. However, broadening is not due to distribution in g values since ΔH_{pp} does not depend on the microwave frequency. Gaussian broadening dominates the 'intrinsic' linewidth. The homogeneous broadening, which have a Lorentzian lineshape, is typically due to relaxation-related mechanism and exchange interactions. Methods to separate different components of the broadening have been developed.[4-9] A few important interactions which are related to line broadening of EPR spectra are discussed in the following sections.

Spin-lattice interaction

The number of electron spins in a typical EPR sample is on the order of 10^{10} or even higher. In the absence of external magnetic field, the two spin states α and β are degenerate. Distributions of the unpaired electrons in the two spin states are equal. In the presence of an external magnetic field H_0, the number of α spins and β spins can be described by the Boltzmann distribution law (Equation 1.4).

$$\frac{n_\alpha}{n_\beta} = \frac{e^{-g\beta H_0/2k_BT}}{e^{g\beta H_0/2k_BT}} \tag{1.4}$$

Here, n_α and n_β are the number of unpaired electrons in the two spin states, k_B is the Boltzmann constant, T is the absolute temperature of the local environment (the 'lattice'). At room temperature, $g\beta H_0/2k_BT \ll 1$, therefore the exponential can be expanded in series, and thus the approximation can be described as Equation 1.5.

$$\frac{n_\alpha}{n_\beta} \simeq \frac{1 - g\beta H_0/2k_BT}{1 + g\beta H_0/2k_BT} \tag{1.5}$$

Hence, in thermal equilibrium the number of unpaired electrons in the lower spin state β is in slight excess. Microwave radiation induces electron transition from the spin state β to α, therefore the system is forced out of equilibrium. Electrons in the α state interact with the lattice and energy transfer from α spins to the lattice leads to electron transitions from α to β, therefore the Boltzmann distribution is restored. The process of recovering equilibrium via spin-lattice interaction is known as spin-lattice relaxation. The rate of this process is characterized by the spin-lattice relaxation time

T_1, which is defined as the time taken to restore the thermal equilibrium by an extent of 1/e (37%). T_1 affects the EPR spectral linewidth. Considering the lifetime of an unpaired electron in a spin state as Δt, the width of the energy level ΔE can be described by the Heisenberg uncertainty principle (Equation 1.6).

$$\Delta E \bullet \Delta t \geq \frac{1}{2}\hbar \tag{1.6}$$

Here, $\hbar$ is the reduced Planck constant. Since $\Delta E = h\Delta\nu = \beta g \Delta H_0$, the resulting linewidth of the corresponding EPR spectrum ΔH can be described as Equation 1.7.

$$\Delta H_0 \geq \frac{h}{2}(\beta g \Delta t)^{-1} \tag{1.7}$$

Evidently, smaller T_1 leads to smaller Δt, and results in larger spectral linewidth. T_1 induced broadening is homogenous and in a Lorentzian lineshape. At low temperature, spin-lattice interaction is much slower which leads to EPR spectra with higher resolution (narrower lines). In fact, temperature dependence of ΔH_{pp} can be used to derive spin-lattice relaxation time. Higher microwave frequency results in faster energy transitions between the spin states, so that spin-lattice interaction is not sufficient to restore the thermal equilibrium. The effect is known as power saturation, which leads to broader spectra and even disappearance of EPR signal.

Spin-spin relaxation

Electron spins not only interact with the lattice but also with each other. Considering a total magnetization vector $\overrightarrow{M}$ as a sum of the magnetic moments of the individual spins (Equation 1.8),

$$\overrightarrow{M} = \sum \mu_i \tag{1.8}$$

In the presence of an external magnetic field H_0 along the z axis and in thermal equilibrium with the lattice, $\overrightarrow{M}$ is directed parallel to the external magnetic field. An electron spin is modulated by the presence of other spins in the vicinity. The additional magnetic field produces a component M_{xy} to the magnetization of the

unpaired electron, which is perpendicular to the external magnetic field H_0. Spins interact with each other and energy transfer within the spin system restores thermal equilibrium in which the magnetization perpendicular to the z axis is zero. The process is characterized by a spin-spin (transverse) relaxation time T_2, which depends on the time it takes to neutralize M_{xy}. Since T_2 is generally smaller than T_1, in the absence of power saturation, EPR linewidth largely depends on spin-spin relaxation (Figure 1.12). T_2 induced line broadening is also Lorentzian.

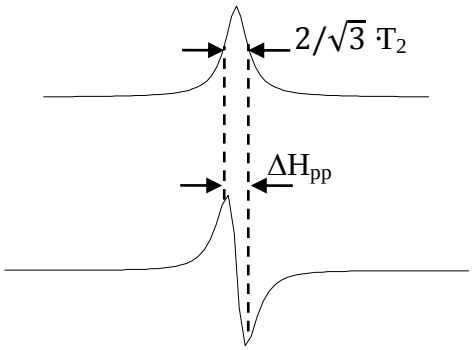

Figure 1. 12. Lorentzian EPR absorption and 1st derivative spectra.

Electron-electron dipolar interaction

Similar to electron-nuclear dipolar interaction, electron spins experience an additional magnetic field provided by the nearby electron spins. The additional magnetic field depends on molecular tumbling, orientation and distance of the nearby electron spins, therefore is anisotropic. A resonance field is contributed by an external magnetic field and an additional magnetic field of the nearby electron spin dipoles. Hence, at a resonance field, the external magnetic field required to induce spin state transition is no longer a fixed value, but have a distribution along the resonance field. Therefore, the resulting EPR spectrum is in fact a superposition of many infinitely narrow lines, and the resulting spectrum is generally in Gaussian lineshape. Dipolar interaction decreases rapidly with increasing spin-spin distance, therefore is weak in magnetically dilute solutions. In more concentrate solutions, dipolar interaction leads to substantial broadening. In solid or viscose samples, the linewidth is much broader than relaxation related broadening. The dipolar

broadening is almost independent of temperature, therefore is considered as the 'intrinsic' linewidth.

Heisenberg exchange interaction

Heisenberg exchange interaction often co-exists with electron-electron dipolar interaction. In comparison with the additional magnetization provided by the dipolar interaction, spin exchange can be classified as a contact interaction. The two electron spins, S_A and S_B, come in close proximity and partial overlapping of molecular orbitals leads to fast relaxation of the spins. The interaction can be explained using a classic model in which the electron spins 'collide' with each other (Figure 1.13).

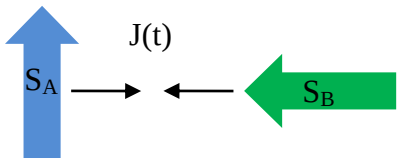

Figure 1. 13. Heisenberg exchange of the two electron spins S_A and S_B. J(t) is the time-dependent inter-spin distance.

The spin exchange Hamiltonian between the two electron spins, S_A and S_B, change in time depending on the inter-spin distance J(t), which is also the isotropic exchange coupling constant (Equation 1.9).

$$H_J = J(t) S_A \bullet S_B \tag{1.9}$$

Inter-molecule spin exchange results in broadening of EPR spectra. For instance, molecular oxygen is paramagnetic. Therefore dissolved O_2 in solution exchanges with the paramagnetic species (*e.g.* nitroxide radical), leading to a Lorentzian broadening proportional to oxygen concentration. This effect is the basis of the EPR oximetry studies described in Chapter 3.

Intra-molecule spin exchange (*e.g.* for biradical) may result in strong coupling of the two electron spins, leading to additional lines in the EPR spectrum. This effect is discussed in Section 1.2.5 (p20).

1.2.4.4. Intensity of EPR spectra

When the shape and linewidth of EPR spectra change, it is impossible to estimate the concentration of the paramagnetic species in the sample from the 1st derivative spectrum recorded or the absorption line. A second integration is needed to transform the 1st derivative spectra to a form, in which the height is proportional to the concentration of the paramagnetic species (Figure 1.14). Practically comparison of the double integration of two EPR spectra, especially if they are from different measurements, is complicated since many factors (*e.g.* position of the sample in the cavity, phase correction, background etc.) need to be considered. But in general, double integration provides an estimation of the spin concentration.

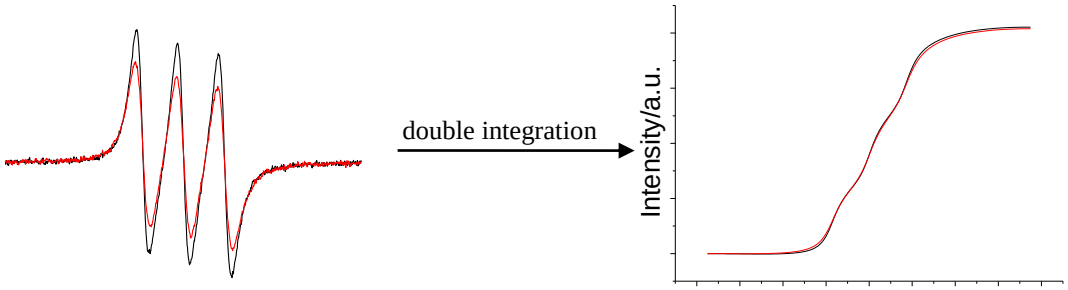

Figure 1. 14. Double integration of spectra with different linewidth results in the same intensity.

1.2.4.5. Dynamics and diffusion

For rapid-tumbling radicals, dipolar interaction average out to zero and hence the resulting EPR spectra are isotropic with g_{iso} and A_{iso}. For instance, nitroxide radicals in a dilute solution yield a triplet EPR spectrum with the three lines of similar height (Figure 1.15a). In the cases where tumbling of the nitroxide radical is restricted (*e.g.* bonded to a metal surface), the high field line is broadened (Figure 1.15b).

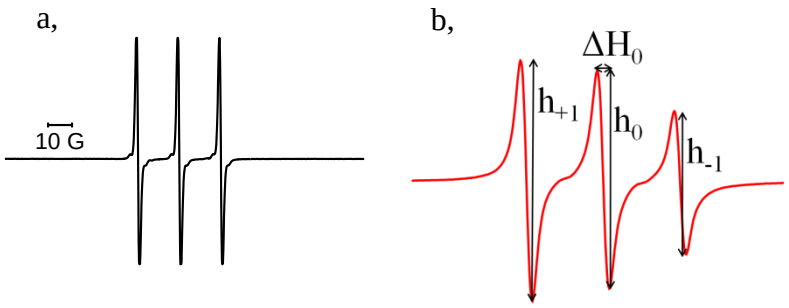

Figure 1. 15. EPR spectra of a free nitroxide radical in its dilute solution (a) and a nitroxide radial bonded to gold nanoparticles (b).

The mobility of a radical can be characterized by a diffusion tensor $\vec{D}$ and Rotational Correlation Time τ_c. The rotational correlation time τ(s) can be obtained by a mathematical calculation (Equation 1.10).

$$\tau(s) = 6.51\times10^{-10}\cdot\Delta H_0\cdot\left(\sqrt{\frac{h_0}{h_{+1}}}+\sqrt{\frac{h_0}{h_{-1}}}-2\right) \qquad (1.10)$$

Here, ΔH_0 is the central line width in gauss, h_{+1}, h_0 and h_{-1} represent the height of the low, middle and high field lines (Figure 1.15b). This well-known method is usually applied to isotropic spectra of nitroxides in which the high field line is broader than the other two lines. By adopting this method, accurate τ values can be obtained in the fast motion regime (*ca.* $\tau_c \leq 4$ ns).

Decrease in mobility (*e.g.* increasing viscosity) results in spectra in the slow motion regime ($\tau_c \geq 4$ ns) (Figure 1.16).

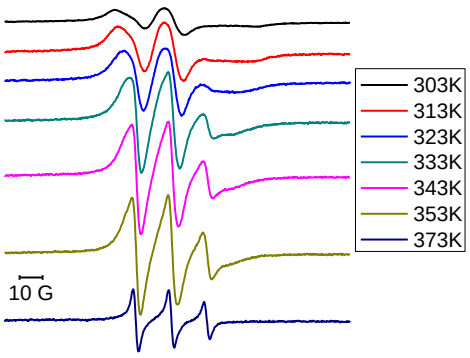

Figure 1. 16. EPR spectra of solid spin-labelled gold nanoparticle at different temperatures.

Further decrease in mobility eventually results in powder pattern spectra (*e.g.* radicals in frozen solution) with anisotropic g and A tensors. Therefore, the resulting EPR spectrum is in fact a superposition of spectra of spins at different orientations.

The diffusion tensor and τ values cannot be measured directly from the slow-motion and powder pattern spectra, but can be obtained from computer simulation. The simulation programs developed by Freed[10] and Stoll[11] are commonly used to acquire diffusion and rotation parameters.

1.2.5. Biradicals

Biradicals have two radical centres connected by a linker. Depending on the size and rigidity of the linker, the different distances between the two radical centres lead to very different exchange interactions. In the cases that the two radical centres are close and frequently 'collide' with each other, additional lines are observed in the EPR spectra of the biradical. For instance, the EPR spectrum of a bisnitroxide disulfide 'DIS3' shows five lines, including two additional exchange peaks as compared to its nitroxide precursor amino-TEMPO (Figure 1.17).

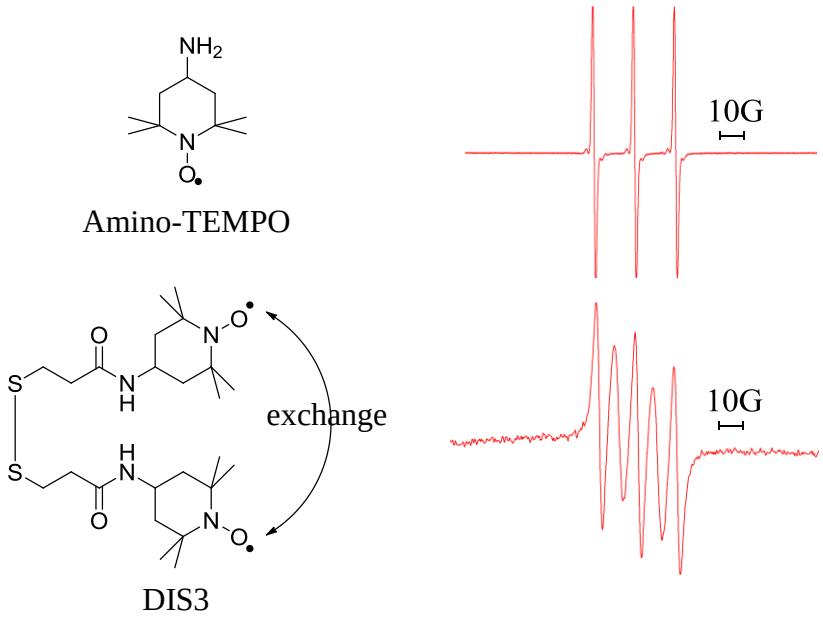

Figure 1. 17.EPR spectra of a bisnitroxide disulfide 'DIS3' in chlorobenzene and its nitroxide radical precursor amino-TEMPO in methylbenzene.

Since the spin-spin interactions includes Heisenberg exchange and dipolar interaction, therefore under high field approximation, the spin Hamiltonian of a pair of coupled electrons can be written as the sum of Zeeman term H_z, exchange term H_J and dipolar term H_{dip} (Equation 1.11).

$$H = H_z + H_J + H_{dip} \tag{1.11}$$

Therefore the overall spin Hamiltonian depends on the relative contribution from Zeeman, exchange and dipolar interactions. In liquid samples, dipolar interaction averages out to zero, hence the EPR spectra depend on the relative ratio of exchange coupling constant J and isotropic hyperfine coupling constant A_{iso} (Figure 1.18[3]). In the cases that the exchange is weak (*e.g.* J≈0), the resulting EPR spectra is dominated by the hyperfine interaction and thus appears to be for a monoradical. In the cases that the exchange coupling constant is substantially larger than hyperfine (i.e. J>>A_{iso}), the EPR spectra appear in a pattern corresponding to two equivalent nuclei with hyperfine coupling constants of $A_{iso}/2$. In the intermediate cases, complicated spectra are observed.

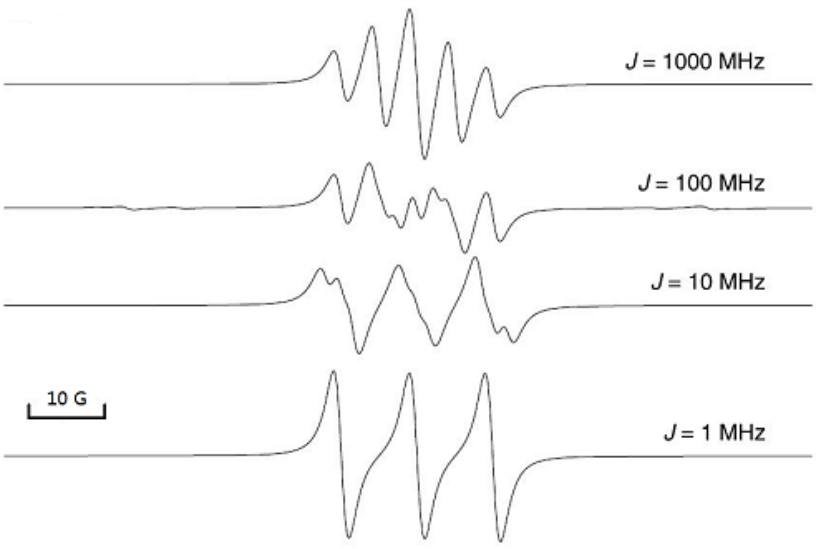

Figure 1. 18. Simulated EPR spectra of a bisnitroxide biradical with different exchange coupling constants.[3]

In solid samples, electron-electron dipolar interaction often dominates the spin Hamiltonian.

1.2.6. Applications of cw-EPR spectroscopy

1.2.6.1. Direct detection

EPR spectroscopy can be utilized to study a number of paramagnetic systems. Most commonly metal complexes, organic radicals and point defects in solids can be directly studied by using EPR spectroscopy. The first published EPR spectrum by Zavoisky[12] in 1944 was in fact a Mn(II) compound. With multi-frequency[13-14] and high field[15-16] EPR, powder spectra of metal complexes[17-19] can provide much structural information. Applications of EPR are also very important in studying radical processes in organic chemistry, including electron transfer[20-25] and polymerization[26-29] which are also involved in the work described in Chapter 3 and 4.

1.2.6.2. Spin labelling

EPR spectroscopy can be used to study diamagnetic systems to which a spin label is introduced. The most common spin labels are nitroxide radicals due to their high persistency, distinctive hyperfine and g values. Detailed introduction of nitroxide chemistry is described in Chapter 3. The structures of some common nitroxide spin probes are shown in Figure 1.19.

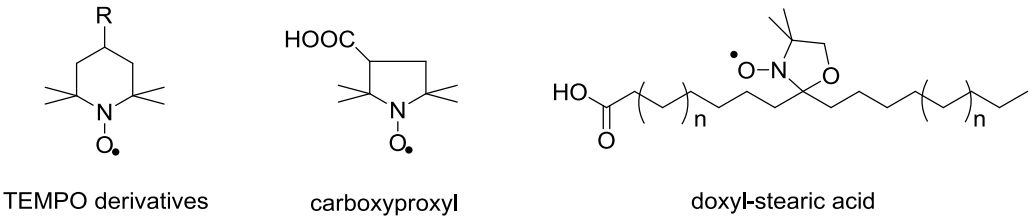

Figure 1. 19. Structures of some common nitroxide spin probes.

Site-directed spin labelling, which was pioneered by Hubbell[30] and co-workers, is an important method in studying biological processes (*e.g.* protein folding) and site-specific dynamics of biological molecules. In combination with pulsed-EPR techniques, the distances in biological systems (*e.g.* distance between protein

domains) can be measured up to 7-8 nm. Spin labelled supramolecular systems is also a popular area of the applications of EPR spectroscopy, including the studies of β-cyclodextrin[31-37] and metal nanoparticles[38-45] by our group. Spin labelled gold nanoparticles are described in Chapter 2.

References:

1. N. M. Atherton, *Principles of Electron Spin Resonance*, Ellis Horwood; PTR Prentice Hall, New York, 1993.
2. A. Schweiger and G. Jeschke, *Principles of Pulse Electron Paramagnetic Resonance*, Oxford University Press, Oxford, 2001.
3. M. Brustolon, ed., *Electron Paramagnetic Resonance: A Practitioner's Toolkit*, John Wiley & Sons, Inc., New Jersey, 2009.
4. A. M. Stoneham, *J. Phys. D: Appl. Phys.*, 1972, **5**, 670-672.
5. H. Floresllamas and H. Yeemadeira, *J. Phys. D: Appl. Phys.*, 1992, **25**, 970-973.
6. R. C. Barklie, M. Collins and S. R. P. Silva, *Phys. Rev. B*, 2000, **61**, 3546-3554.
7. A. I. Smirnov, *J. Magn. Reson.*, 2008, **190**, 154-159.
8. A. I. Smirnov and R. L. Belford, *J. Magn. Reson., Ser A*, 1995, **113**, 65-73.
9. H. J. Halpern, M. Peric, C. Yu and B. L. Bales, *J. Magn. Reson., Ser A*, 1993, **103**, 13-22.
10. D. J. Schneider and J. H. Freed, in *Biological Magnetic Resonance*, eds. L. J. Berliner and J. Reuben, Plenum Press, New York, Editon edn., 1989, pp. 1-76.
11. S. Stoll and A. Schweiger, *J. Magn. Reson.*, 2006, **178**, 42-55.
12. E. Zavoisky, *J. Phy.-USSR*, 1944, **8**, 377-380.
13. J. A. Fee, D. Sanders, C. E. Slutter, P. E. Doan, R. Aasa, M. Karpefors and T. Vanngard, *Biochem. Biophys. Res. Commun.*, 1995, **212**, 77-83.
14. R. B. Clarkson, A. I. Smirnov, T. I. Smirnova, H. Kang, R. L. Belford, K. Earle and J. H. Freed, *Mol. Phys.*, 1998, **95**, 1325-1332.
15. J. Krzystek, S. A. Zvyagin, A. Ozarowski, S. Trofimenko and J. Telser, *J. Magn. Reson.*, 2006, **178**, 174-183.
16. J. Krzystek, A. Ozarowski and J. Telser, *Coord. Chem. Rev.*, 2006, **250**, 2308-2324.
17. T. Spalek, P. Pietrzyk and Z. Sojka, *J. Chem. Inf. Model.*, 2005, **45**, 18-29.
18. D. H. Kim, R. D. Britt, M. P. Klein and K. Sauer, *Biochemistry*, 1992, **31**, 541-547.

19. P. Chaudhuri, M. Winter, B. P. C. Dellavedova, E. Bill, A. Trautwein, S. Gehring, P. Fleischhauer, B. Nuber and J. Weiss, *Inorg. Chem.*, 1991, **30**, 2148-2157.
20. L. Noodleman, C. Y. Peng, D. A. Case and J. M. Mouesca, *Coord. Chem. Rev.*, 1995, **144**, 199-244.
21. H. Michel, J. Behr, A. Harrenga and A. Kannt, *Annu. Rev. Biophys. Biomol. Struct.*, 1998, **27**, 329-356.
22. H. Kurreck and M. Huber, *Angew. Chem. Int. Ed.*, 1995, **34**, 849-866.
23. M. Kurmoo, A. W. Graham, P. Day, S. J. Coles, M. B. Hursthouse, J. L. Caulfield, J. Singleton, F. L. Pratt, W. Hayes, L. Ducasse and P. Guionneau, *J. Am. Chem. Soc.*, 1995, **117**, 12209-12217.
24. D. C. Hurum, A. G. Agrios, K. A. Gray, T. Rajh and M. C. Thurnauer, *J. Phys. Chem. B*, 2003, **107**, 4545-4549.
25. K. Brettel, *BBA-Bioenergetics*, 1997, **1318**, 322-373.
26. J. Virtanen, H. Lemmetyinen and H. Tenhu, *Polymer*, 2001, **42**, 9487-9493.
27. K. Matyjaszewski and A. Kajiwara, *Macromolecules*, 1998, **31**, 548-550.
28. A. Kajiwara, K. Matyjaszewski and M. Kamachi, *Macromolecules*, 1998, **31**, 5695-5701.
29. D. C. Doetschman, R. C. Mehlenbacher and D. Cywar, *Macromolecules*, 1996, **29**, 1807-1816.
30. W. L. Hubbell, D. S. Cafiso and C. Altenbach, *Nature Struct. Biol.*, 2000, **7**, 735-739.
31. V. Chechik and G. Ionita, *Org. Biomol. Chem.*, 2006, **4**, 3505-3510.
32. G. Ionita, M. Florent, D. Goldfarb and V. Chechik, *J. Phys. Chem. B*, 2009, **113**, 5781-5787.
33. G. Ionita and V. Chechik, *Org. Biomol. Chem.*, 2005, **3**, 3096-3098.
34. G. Ionita and V. Chechik, *PCCP*, 2010, **12**, 6956-6960.
35. G. Ionita, A. Caragheorgheopol, H. Caldararu, L. Jones and V. Chechik, *Org. Biomol. Chem.*, 2009, **7**, 598-602.
36. G. Ionita, V. Meltzer, E. Pincu and V. Chechik, *Org. Biomol. Chem.*, 2007, **5**, 1910-1914.
37. V. Chechik and G. Ionita, *New J. Chem.*, 2007, **31**, 1726-1729.
38. V. Chechik, H. J. Wellsted, A. Korte, B. C. Gilbert, H. Caldararu, P. Ionita and A. Caragheorgheopol, *Faraday Discuss.*, 2004, **125**, 279-291.

39. P. Ionita, B. C. Gilbert and V. Chechik, *Angew. Chem. Int. Ed.*, 2005, **44**, 3720-3722.

40. P. Ionita, A. Caragheorgheopol, B. C. Gilbert and V. Chechik, *Langmuir*, 2004, **20**, 11536-11544.

41. P. Ionita, J. Wolowska, V. Chechik and A. Caragheorgheopol, *J. Phys. Chem. C*, 2007, **111**, 16717-16723.

42. P. Ionita, A. Volkov, G. Jeschke and V. Chechik, *Anal. Chem.*, 2008, **80**, 95-106.

43. P. Ionita, M. Conte, B. C. Gilbert and V. Chechik, *Org. Biomol. Chem.*, 2007, **5**, 3504-3509.

44. P. Ionita, A. Caragheorgheopol, B. C. Gilbert and V. Chechik, *J. Am. Chem. Soc.*, 2002, **124**, 9048-9049.

45. P. Ionita, A. Caragheorgheopol, B. C. Gilbert and V. Chechik, *J. Phys. Chem. B*, 2005, **109**, 3734-3742.